JOURNAL of the MEXICAN CHEMICAL SOCIETY

https://www.jmcs.org.mx/

Article

Open Access

J. Mex. Chem. Soc. **2026**, *70(1):e2508*

Received June 25th, 2025
Accepted November 24th, 2025

http://dx.doi.org/10.29356/jmcs.v70i1.2508
e-location ID: 2508

Keywords:
Cocrystal; π-π interactions; H-bonding; Hirshfeld surface; influence of F atoms

Palabras clave:
Cocristal; interacciones π-π; enlaces de hidrógeno; superficie de Hirshfeld; influencia de los átomos de F

***Corresponding author:**
Jesús Valdés-Martínez
email: jvaldes@iquimica.unam.mx

ISSN-e 2594-0317

Influence of Fluorine Substitution on π-π Stacking and Molecular Packing in Schiff Base Cocrystals

Mónica Hernández-Vergara, Addi Dana Sánchez-Pacheco, Simón Hernández-Ortega, Jesús Valdés-Martínez*

Instituto de Química, Universidad Nacional Autónoma de México, Circuito Exterior, Ciudad Universitaria, 04510 Coyoacán, Ciudad de México, México.

Abstract. In this study, we investigate the role of fluorine atom positioning in the supramolecular organization, π-π stacking interactions, and molecular packing of Schiff base cocrystals. Three cocrystals, each containing *(E)-N*-(trifluoroaniline)-1-(4-pyridinyl)-methanimine with *p*-dimethylaminobenzoic acid, were synthesized with fluorine atoms positioned at different sites on the aromatic rings (2,3,4; 2,4,5; and 3,4,5). IR spectroscopy confirmed the formation of cocrystals, highlighting the presence of strong O–H···N hydrogen bonds. Crystal structure analysis revealed that fluorination at the 2,3,4 positions led to parallel molecular packing, whereas fluorination at the 2,4,5 and 3,4,5 positions resulted in oblique-angle packing. Hirshfeld surface analysis and density functional theory (DFT) calculations demonstrated that π-π interactions, particularly between the pyridine and trifluorinated aromatic rings, are energetically significant and often surpass the strength of hydrogen bonds. These findings underscore the importance of fluorine atom positioning in determining the molecular packing and provide valuable insights into the design of cocrystals through the strategic manipulation of intermolecular forces.

Resumen. En este estudio investigamos el papel de la posición de los átomos de flúor en la organización supramolecular, las interacciones de apilamiento π-π y el empaquetamiento molecular de cocristales de una base de Schiff. Tres cocristales, cada uno conteniendo (E)-N-(trifluoroanilina)-1-(4-piridinil)-metanimina con ácido p-dimetilaminobenzóico,

J. Mex. Chem. Soc. **2026**, *70(1):e2508*
Regular Issue

ISSN-e 2594-0317

fueron sintetizados con átomos de flúor posicionados en diferentes sitios de los anillos aromáticos (2,3,4; 2,4,5; y 3,4,5). La espectroscopía IR confirmó la formación de cocristales, destacando la presencia de fuertes enlaces de hidrógeno O−H···N. El análisis de las estructuras cristalinas reveló que el patrón de fluoración en las posiciones 2,3,4 condujo a un empaquetamiento molecular paralelo, mientras que la fluoración en las posiciones 2,4,5 y 3,4,5 resultó en arreglos de empaquetamiento oblicuos. El análisis de superficie de Hirshfeld y los cálculos con la teoría del funcional de la densidad (DFT) demostraron que las interacciones π-π, en particular entre la piridina y los anillos aromáticos trifluorados, son energéticamente significativas y, a menudo, superan la fuerza de los enlaces de hidrógeno. Estos hallazgos resaltan la importancia de la posición de los átomos de flúor en la determinación del empaquetamiento molecular y ofrecen información valiosa para el diseño de cocristales mediante la manipulación estratégica de las fuerzas intermoleculares.

Introduction

The design and synthesis of cocrystals are of great interest in fundamental chemistry and pharmaceutical research, as they provide a means to tailor solid-state properties [1]. Successful cocrystal design depends on predictable intermolecular interactions, governed by both the strength and the directionality of the forces involved. The design and synthesis of cocrystals are of great interest in both fundamental chemistry and pharmaceutical applications, as they can tailor solid-state properties [1]. A key aspect of cocrystal design relies on reliable intermolecular interactions, which depend on both the strength and directionality of the forces involved. While hydrogen and halogen bonding are well understood owing to their predictable directionality, interactions between aromatic rings, particularly π-π stacking, are less explored. Despite their relatively low strength and less predictable nature, aromatic interactions commonly occur in crystal structures and biological systems [2-5], warranting further investigation to harness their full potential in crystal engineering.

We utilize small molecules to investigate intermolecular interactions to design and synthesize solid compounds (Scheme 1). These molecules exhibit a range of intermolecular forces, allowing for comparison of their competitive nature [6]. Because of their multiple reactive sites, they are referred to as multifunctional supramolecular molecules. Similar small molecules, consisting of two aromatic rings linked by an -X=Y- group (where X and Y can be either C or N), have been extensively studied. Ojala and his group, for instance, investigated "bridge-flipped" isomerism in benzilideneanilines and phenylhydrazones [7-9]. Additionally, [2+2] photodimerization of stilbazoles in the solid state has been studied using small molecules as linear templates [10-15], as well as carboxylic acids, coordination compounds, and pseudorotaxane-like metal-organic frameworks (MOFs) [15-18]. These systems have also been explored for applications in nonlinear optics (NLO) [19] and liquid crystals [20-21].

In this study, we investigate the impact of fluorine atom positioning on aromatic rings and its influence on π-π interactions and molecular packing within cocrystals. Building on our previous work with perhalogenated molecules [22,23], we now focus on systems containing three fluorine atoms to investigate how their specific placement affects the supramolecular organization. By comparing cocrystals with different fluorination patterns, we aim to understand how these interactions affect crystal packing. This study offers insight into the competitive forces governing the molecular arrangement of fluorinated aromatic systems. Specifically, we address the following question: Will these cocrystals exhibit strong π interactions similar to those observed in molecules with five halogens? Will an imine hydrogen atom form C-H···F hydrogen bonds? How will the positioning of fluorine atoms affect molecular packing within the crystal? To answer these questions, we analyzed the crystal structures of three Schiff base cocrystals with fluorine atoms at different positions: 2,3,4 (***1***), 2,4,5 (***2***), and 3,4,5 (***3***), each with p-dimethylaminobenzoic acid (Scheme 1). Hirshfeld surface analysis and DFT calculations were also performed to gain deeper insights into the nature and energetic contributions of these interactions to molecular packing.

http://dx.doi.org/10.29356/jmcs.v70i1.2508

J. Mex. Chem. Soc. **2026**, *70(1):e2508*
Regular Issue

ISSN-e 2594-0317

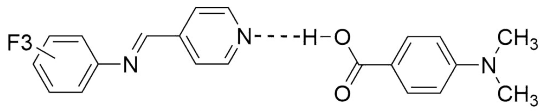

F3=2,3,4; 3,4,5; 2,4,5

Scheme 1. Structure of the cocrystals ***1*** (F3 = 2,3,4), ***2*** (F3 = 3,4,5), and ***3*** (F3 = 2,4,5).

Experimental

The reagents 2,3,4-trifluoroaniline, 2,4,5-trifluoroaniline, 3,4,5-trifluoroaniline, 4-(dimethylamino)benzoic acid, 4-pyridinecarboxaldehyde, toluene, and acetic acid were purchased from commercial sources and used without further purification. Melting points (uncorrected) were determined using a Fischer-Johns Mel-Temp melting point apparatus. Infrared spectra were collected using a Nicolet 380 FT-IR instrument (ATR). ^{1}H, ^{13}C, and ^{19}F NMR spectra were obtained using an Oxford NMR 300 MHz spectrometer. Mass spectra were recorded on a JEOL JMS-T100LC spectrometer using the DART (Direct Analysis in Real Time) technique.

Synthesis and crystallization

The (*E*)-N-(2,3,4-trifluoroaniline)-1-(4-pyridinyl)-methanimine, (***234-F***), (*E*)-N-(2,4,5-trifluoroaniline)-1-(4-pyridinyl)-methanimine (***245-F***), and (*E*)-N-(3,4,5-trifluoroaniline)-1-(4-pyridinyl)-methanimine, (***345-F***), were obtained from an equimolar reaction of 4-pyridinecarboxaldehide and the corresponding trifluoroaniline as previously reported.

The details of the synthesis and spectroscopic characterization are provided in the Supplementary Material [24].

Cocrystals were obtained by heating equimolecular amounts of the imine and 4-(dimethylamino)benzoic acid in a 4 mL vial with a heating gun until the solids melted, and then cooling the melt to room temperature. The compounds were recrystallized in toluene to obtain crystals for single-crystal X-ray diffraction studies.

X-ray crystallography

Single crystals of ***1-3***, obtained upon recrystallization, were mounted on top of a glass fiber using an epoxy resin. Crystallographic data were collected using monochromatic Mo Kα (λ = 0.71073 Å) radiation at 293(2) K on a Bruker D8 Venture 208039-01 κ-geometry diffractometer. Data were collected using APEX3[25], reduced with SAINT, and corrected for absorption with SADABS [25]. The structures were solved by direct methods using SHELXT [26] and refined against F^2 by full-matrix least squares with SHELXL [27]. All atoms, except hydrogen, were located in a difference electron density map and refined anisotropically. Analysis of the electron density map and the geometry of each atomic scatterer allowed each atom to be assigned. Hydrogen atoms were included at geometrically idealized positions and refined with the riding model, with U_{iso} tied to the parent atom. Hydrogen atoms associated with the imine nitrogen were found from the Fourier difference map and were given an isotropic displacement of 1.2 Ueq of the parent atom. The OH hydrogens were assigned an isotropic displacement of 1.5 Ueq relative to the parent atom. The electron density neighboring the N and O atoms, along with their distance and bond angles, were observed, assigned, and refined as hydrogen atoms. The geometric parameters were obtained using Platon [28] and Mercury [29]. Figures were elaborated using X-seed 4 [30]. Details of the measured crystals, their data collection, and refining parameters are given in Table S1 of the Supplementary Material.

Crystal data for 1: $C_{21}H_{18}F_3N_3O_2$, M = 401.38 g mol^{-1}, yellow Prism, 0.370 × 0.197 × 0.079 mm^3, monoclinic, space group $P2_1/n$ (No. 14), a = 6.4190(3), b = 13.6608(8), c = 21.2266(11) Å, β = 97.481(2) °, V = 1845.49(17) Å^3, Z = 4, D_c = 1.445 g cm^{-3}, F_{000} = 832, Bruker APEX2 CCD area detector, MoKα radiation, λ = 0.71073 Å, T = 150(2) K, $2\theta_{max}$ = 50.6º, 10543 reflections collected, 3342 unique (R_{int} = 0.0949). Final *GooF* = 1.033, $R1$ = 0.0477, $wR2$ = 0.1086, R indices based on 2246 reflections with $I > 2\sigma(I)$ (refinement on F^2), 268 parameters, 1 restraint. Lp and absorption corrections were applied, μ = 0.115 mm^{-1}.

http://dx.doi.org/10.29356/jmcs.v70i1.2508

J. Mex. Chem. Soc. **2026**, *70(1):e2508*
Regular Issue

ISSN-e 2594-0317

Crystal data for 2: $C_{21}H_{18}F_3N_3O_2$, M = 401.38 g mol^{-1}, yellow Prism, 0.509 × 0.237 × 0.205 mm^3, monoclinic, space group *C*2/*c* (No. 15), a = 30.5815(16), b = 6.4400(3), c = 20.2973(11) Å, β = 115.4555(8)°, V = 3609.4(3) Å^3, Z = 8, D_c = 1.477 g cm^{-3}, F_{000} = 1664, Bruker APEX-II CCD, MoKα radiation, λ = 0.71073 Å, T = 100(2) K, 2θ_{max} = 54.1º, 17940 reflections collected, 3954 unique (R_{int} = 0.0366). Final *GooF* = 1.048, $R1$ = 0.0414, $wR2$ = 0.1149, R indices based on 3426 reflections with $I > 2\sigma(I)$ (refinement on F^2), 267 parameters, 1 restraint. Lp and absorption corrections were applied, μ = 0.118 mm^{-1}.

Crystal data for 3: $C_{21}H_{18}F_3N_3O_2$, M = 401.38 g mol^{-1}, colorless Prism, 0.360 × 0.125 × 0.117 mm^3, monoclinic, space group *C*2/*c* (No. 15), a = 26.968(3), b = 6.7750(8), c = 22.610(3) Å, β = 115.039(2)°, V = 3742.8(8) Å^3, Z = 8, D_c = 1.425 g cm^{-3}, F_{000} = 1664, Bruker APEX2 CCD area detector, MoKα radiation, λ = 0.71073 Å, T = 150(2) K, 2θ_{max} = 50.5º, 13112 reflections collected, 3374 unique (R_{int} = 0.0902). Final *GooF* = 1.037, $R1$ = 0.0448, $wR2$ = 0.0986, R indices based on 2712 reflections with $I > 2\sigma(I)$ (refinement on F^2), 268 parameters, 1 restraint. Lp and absorption corrections were applied, μ = 0.114 mm^{-1}.

Crystallographic data, including the supplementary crystallographic data for this paper, were deposited in the Cambridge Crystallographic Data Centre (CCDC) under the numbers CCDC 2392729-2392731. These data can be obtained free of charge via http://www. ccdc.cam.ac.uk/conts/retrieving.html (or from the Cambridge Crystallographic Data Centre, 12, Union Road, Cambridge CB2 1EZ, UK; fax: + 441223 336033).

Computational studies

We use the CrystalExplorer 21 software to calculate Hirshfeld surfaces for the compounds.[31] The study began by calculating the Hirshfeld surface [32] and the 2D fingerprints.[33] Hirshfeld surfaces were mapped with the d_{norm} and Shape Index properties. The single-point energy for pairs of molecules was calculated using their crystal geometry with the M06-2X functional and the 6-31+G** basis set, as implemented in Spartan 20 (Wavefunction, Inc., Irvine, CA, USA). For the DFT calculations, we used the default values for the grid and SCF convergence criterion.

Results and discussion

The asymmetric units of ***1–3*** (Fig. 1) consist of an imine molecule and a 4-(dimethylamino)benzoic acid (***BzAc***) molecule. The imines are present as the *E* isomer, forming an (N(py)···O-H) hydrogen bond with ***BzAc***. In ***1–3***, the trifluorinated aromatic ring (^{F}Ar), pyridine ring (py), and benzene ring are not in the same plane, see Table 1.

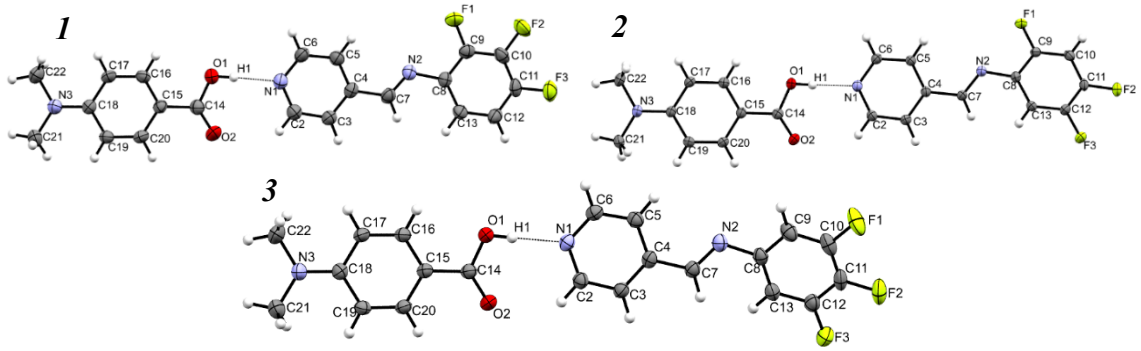

Fig. 1. Asymmetric unit plots of ***1 – 3*** with scheme numbering. Displacement ellipsoids are drawn at the 50 % probability level, and hydrogen atoms at an arbitrary size.

J. Mex. Chem. Soc. **2026**, *70(1):e2508*
Regular Issue

ISSN-e 2594-0317

Table 1. Angle between the aromatic rings in ***1*** **–** ***3***, (º).

	Cg(1)$^{(i)}$-Cg(2)$^{(ii)}$	Cg(1)-Cg(3)$^{(iii)}$	Cg(2)-Cg(3)
1	8.67(10)	30.27(9)	38.93(9)
2	29.49(8)	5.77(8)	29.06(8)
3	22.17(7)	2.09(7)	23.86(7)

(i) Cg(1): N1/C2-C6, (ii) Cg(2): C8-C13; (III) Cg(3): C15-C20

To analyze the supramolecular structure of the cocrystals, we employed a combination of geometric parameters and Hirshfeld surface analysis, including d_{norm} and Shape Index mapping, as well as 2D fingerprint plots.

Fig. 2 presents the 2D fingerprint plots derived from the Hirshfeld surfaces for each molecule, highlighting the distinct differences that reflect the variations in the crystal structures. Column (a) shows the overall fingerprints for molecules ***234-F***, ***245-F***, ***345-F***, and their corresponding ***BzAc***, and the delineated interactions for HN/NH, HF/FH, and OH/HO are shown in columns b, c, and d, respectively. The top row for each cocrystal shows the fingerprints for the imine, while the second row displays the fingerprints for the benzoic acid. Tables with the percentage contribution to the total surface area of each delineated interaction are presented in the Supplementary Material.

The characteristic wing-like features in the fingerprint plots display an asymmetric long peak that corresponds to the N(py)···H—O(***BzAc***) hydrogen bond in the trifluoro imines and O—H(***BzAc***)···N(py) in the ***BzAc*** structures. In all cases, this interaction exhibited the shortest $d_i \cdots d_e$ (internal···external) distance in ***1-3***, suggesting a strong hydrogen bond.

The H···F interactions show two main contributions: H(imine)···F(imine) and F(imine)···H(***BzAc***). However, as expected, ***BzAc*** only displays H(***BzAc***)···F(imine) contacts. In cocrystal ***1***, this interaction presents the shortest distance, indicating that it may be more significant in ***1*** than in ***2*** and ***3***.

Since the imines lack an oxygen atom, they exhibit only H(imine)···O(***BzAc***) interactions. Conversely, the ***BzAc*** component displays two O(***BzAc***)···H(imine) peaks, but only one falls within the expected hydrogen bonding distance.

These findings highlight the crucial interplay of the intermolecular interactions between both molecular components in each cocrystal.

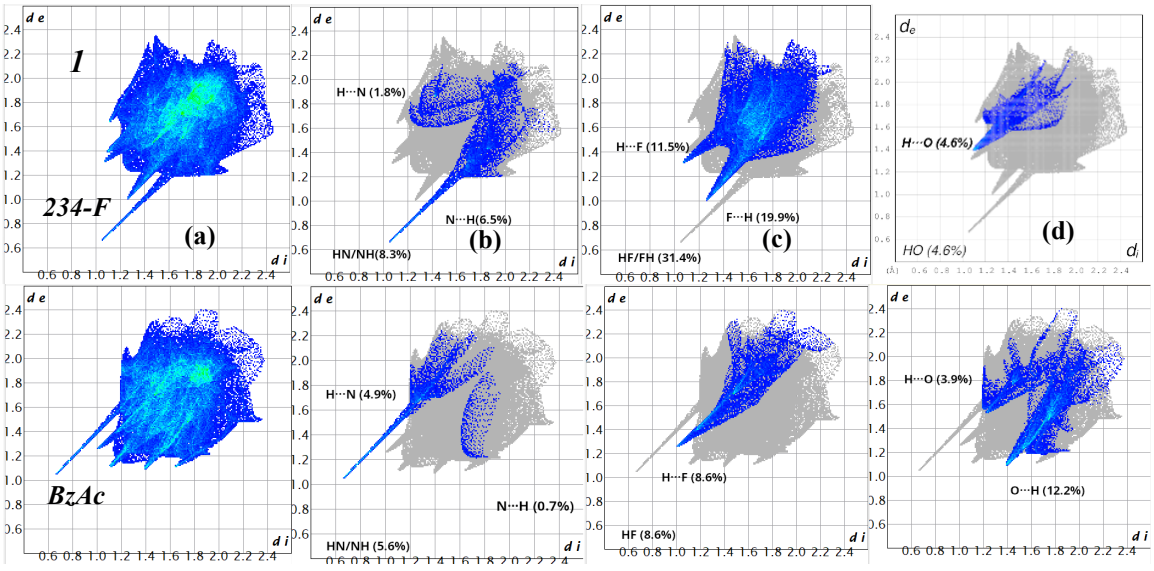

http://dx.doi.org/10.29356/jmcs.v70i1.2508

J. Mex. Chem. Soc. **2026**, *70(1):e2508*
Regular Issue

ISSN-e 2594-0317

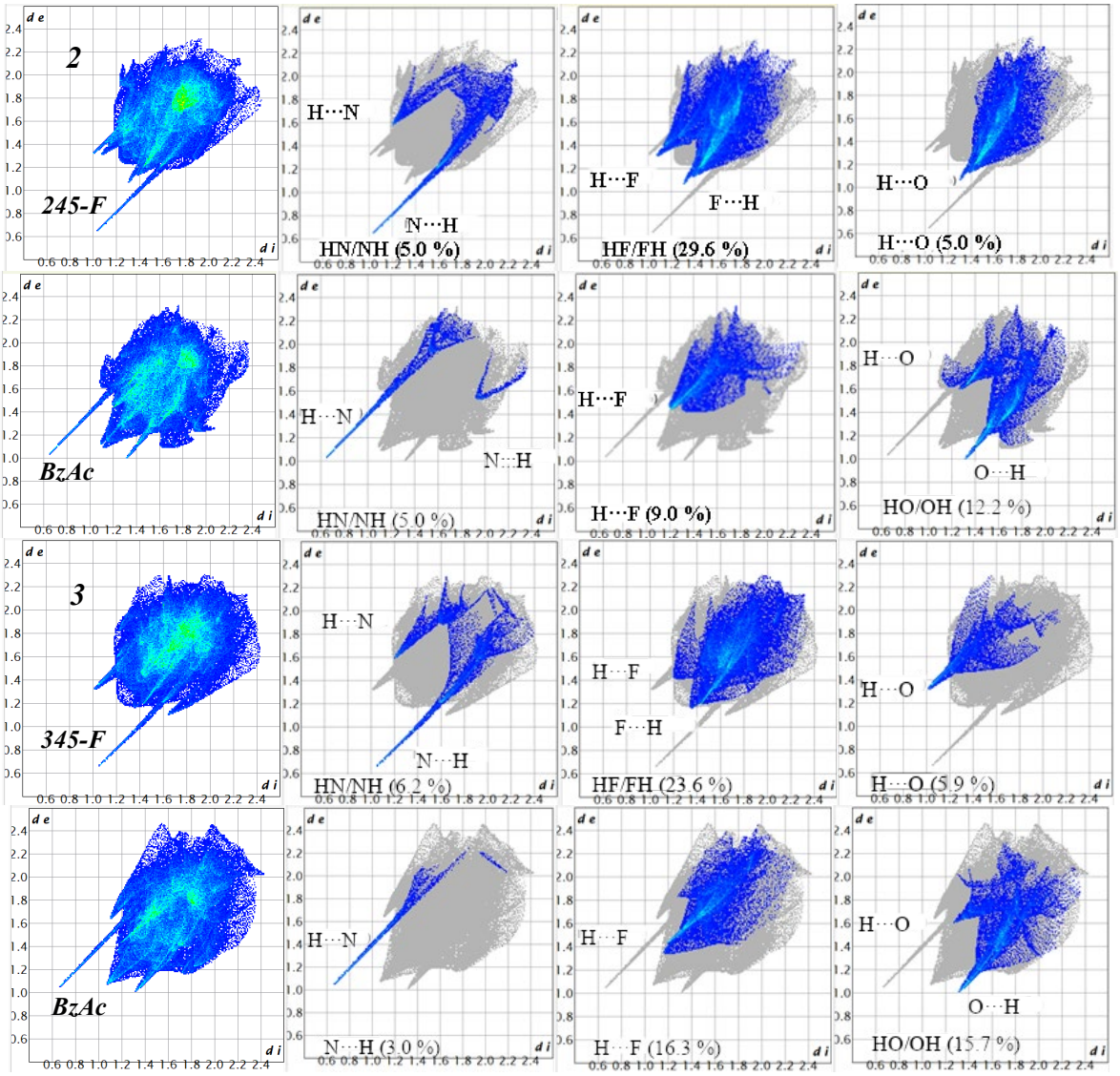

Fig. 2. Overall two-dimensional fingerprint plots for **(a)** molecules ***234-F***, ***245-F***, ***345-F***, and the corresponding ***BzAc*** acid molecules, and those delineated into **(b)** H···N/N···H, **(c)** H···F/F···H, and **(d)** H···O/O···H contacts, with the percentage contributions specified within each plot.

The Hirshfeld surfaces mapped with the d_{norm} parameter helped identify directional intermolecular interactions. Fig. 3 shows the Hirschfeld surfaces for cocrystals ***1*** **–*3***. In all of them, the surfaces show intense red spots indicative of strong interactions for the O-H(imine)···N(py) H bonds. The less intense spots correspond to C-H···O and C-H···F interactions.

A geometric analysis of the structures agrees with the previous results. Table 2 presents the intermolecular distances and angles observed in the cocrystals, and Fig. 4 shows the intermolecular interactions.

http://dx.doi.org/10.29356/jmcs.v70i1.2508

J. Mex. Chem. Soc. **2026**, *70(1):e2508*
Regular Issue

ISSN-e 2594-0317

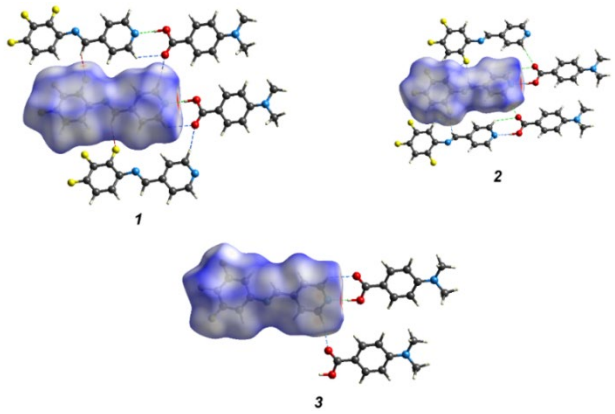

Fig. 3. Hirshfeld surfaces mapped with d_{norm} for ***1*** – ***3***, showing O-H···N, C-H···F, and C-H···O interactions.

Table 3. Selected hydrogen-bond parameters

D*—H···*A	***D*—H (Å)**	**H···*A* (Å)**	***D*···*A* (Å)**	***D*—H···*A* (°)**
1				
C2—H2···O2^{i}	0.95	2.58	3.261 (2)	128.8
C6—H6···O2^{ii}	0.95	2.60	3.393 (2)	141.5
C7—H7···F1^{iii}	0.95	2.49	3.291 (2)	142.0
O1—H1···N1^{iv}	0.860 (9)	1.84 (1)	2.698 (2)	174 (2)
C21—H21B···F3^{v}	0.98	2.35	3.141 (2)	137.4
C22—H22C···F3^{vi}	0.98	2.63	3.356 (3)	130.9
2				
O1—H1···N1^{vii}	0.853 (9)	1.82 (1)	2.669 (2)	177 (2)
C2—H2···O2^{viii}	0.95	2.61	3.296 (2)	129.3
C6—H6···O2^{ix}	0.95	2.44	3.335 (2)	156.2
C7—H7···F1^{x}	0.95	2.48	3.254 (2)	138.4
C13—H13···F1^{x}	0.95	2.64	3.475 (2)	147.6
3				
O1—H1···N1^{xi}	0.869 (9)	1.837 (9)	2.706 (2)	179 (2)
C2—H2···O2^{ix}	0.95	2.42	3.145 (2)	132.5
C6—H6···O2^{viii}	0.95	2.51	3.360 (2)	148.4
C22—H22A···F2^{xii}	0.98	2.56	3.059 (2)	111.5

Symmetry code(s): (i) -*x*+1/2, *y*+1/2, -*z*+1/2; (ii) -*x*+3/2, *y*+1/2, -*z*+1/2; (iii) *x*-1, *y*, *z*; (iv) -*x*+1/2, *y*-1/2, *z*+1/2;(v)-*x*+5/2,*y*-1/2,-*z*+3/2; (vi) -*x*+3/2, *y*-1/2, -*z*+3/2; (vii) *x*-1/2, *y*-1/2, *z*; (viii) *x*+1/2, *y*+1/2, *z*; (ix) *x*+1/2, *y*-1/2, *z*; (x) *x*, *y*+1, *z*; (xi) *x*-1/2, *y*+1/2, *z*; (xii) *x*, -*y*+1, *z*-1/2.

http://dx.doi.org/10.29356/jmcs.v70i1.2508

J. Mex. Chem. Soc. **2026**, *70(1):e2508*
Regular Issue

ISSN-e 2594-0317

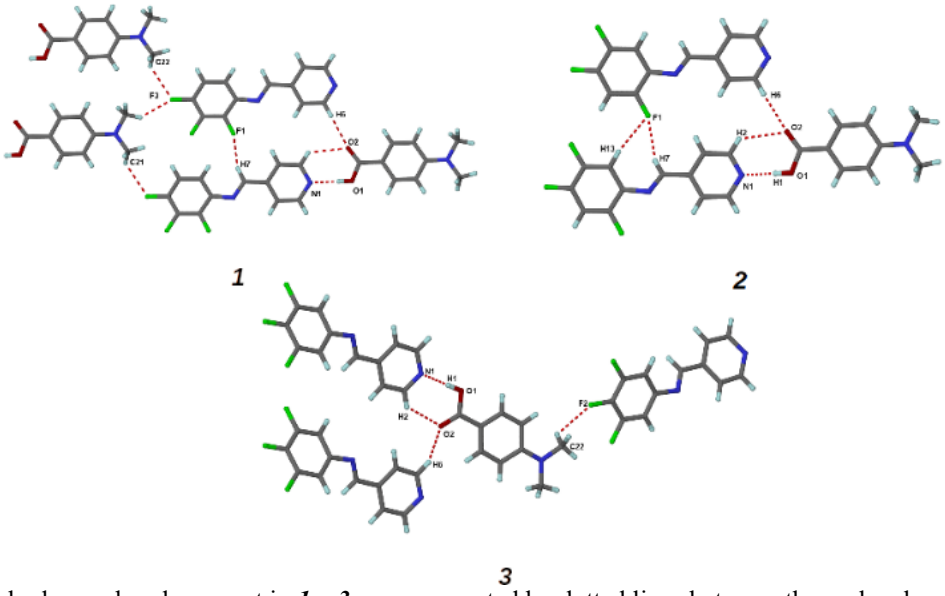

Fig. 4. The hydrogen bonds present in ***1 – 3*** are represented by dotted lines between the molecules.

Shape Index mapping of the Hirshfeld surface enabled us to identify stacking π-π interactions between the aromatic rings. When these interactions are present, complementary red and blue triangles appear on the surface of the aromatic rings, as shown in Fig. 5 for compound ***1*** (see the Supplementary Data for compounds ***2*** and ***3***). Table 3 provides the relevant parameters, and Fig. 6 illustrates the π-π interactions observed in these systems.

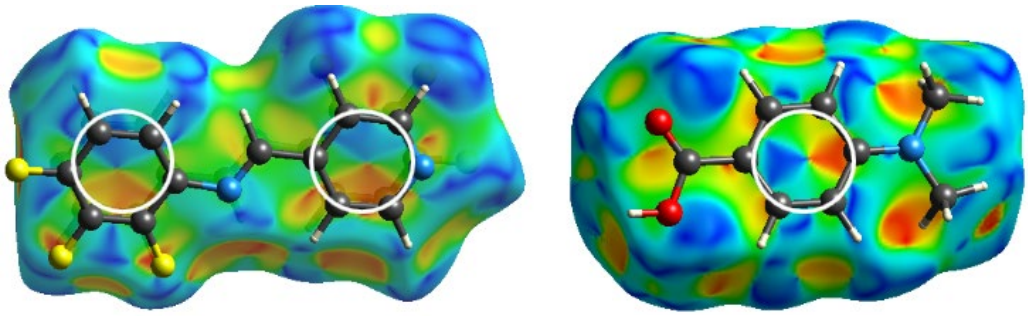

Fig. 5. Hirshfeld surfaces for ***234-F*** imine and benzoic acid. The red and blue triangles on the aromatic rings indicate π-π interactions.

Table 4. Parameters of π–π interactions between the aromatic rings in ***1*** – ***3***.

Cg(I)···Cg(J)[a]	**Symm. Op.**	**Cg···Cg (Å)**	**α[b]**	**Slippage (Å)[c]**
1				
Cg1 - Cg2	1-x,2-y,1-z	3.597(1)	8.7(1)	0.617
Cg3 - Cg3	2-x,1-y,1-z	3.765(1)	0.03(9)	1.155

http://dx.doi.org/10.29356/jmcs.v70i1.2508

J. Mex. Chem. Soc. **2026**, *70(1):e2508*
Regular Issue

ISSN-e 2594-0317

Cg(I)···Cg(J)[a]	Symm. Op.	Cg···Cg (Å)	α[b]	Slippage (Å)[c]
2				
Cg1···Cg1	3/2-x,3/2-y,1-z	3.6550(8)	0.3(7)	1.283
Cg1···Cg2	3/2-x,1/2+y,3/2-z	3.6523(8)	3.19(7)	1.367
Cg2···Cg1	3/2-x,-1/2+y,3/2-z	3.6524(8)	3.19(7)	1.458
Cg3···Cg3	1-x,2-y,1-z	3.7090(9)	0.03(7)	1.072
3				
Cg1···Cg1	3/2-x,1/2-y,1-z	3.686(1)	0.02(7)	1.699
Cg1···Cg2	3/2-x,-1/2+y,3/2-z	3.616(1)	5.85(8)	1.230
Cg3···Cg3	1-x,-y,1-z	3.968(1)	0.02(8)	1.823

[a] Cg Ring centroids: Cg(1): N1/C2-C6, Cg(2): C8-C13; Cg(3): C15-C20,
[b] Dihedral angle between planes I and J.
[c] Slippage = distance between Cg(I) and the perpendicular projection of Cg(J) on ring I (Å).

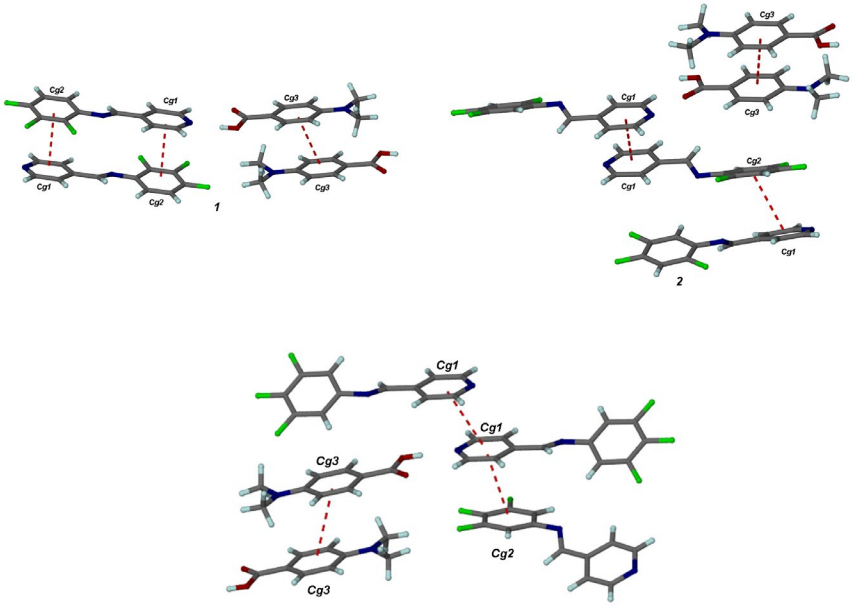

Fig. 6. Interactions involving aromatic rings in compounds ***1–3***.

Fig. 7 shows how the molecules are organized into planes, which are then stacked on top of each other to form the crystal structure. In compound ***1***, the molecules pack in a relatively linear manner. However, in compounds ***2*** and ***3***, the interacting rings are arranged at an angle, creating the pattern shown in Fig 6 (2c).

http://dx.doi.org/10.29356/jmcs.v70i1.2508

J. Mex. Chem. Soc. **2026**, *70(1):e2508*
Regular Issue

ISSN-e 2594-0317

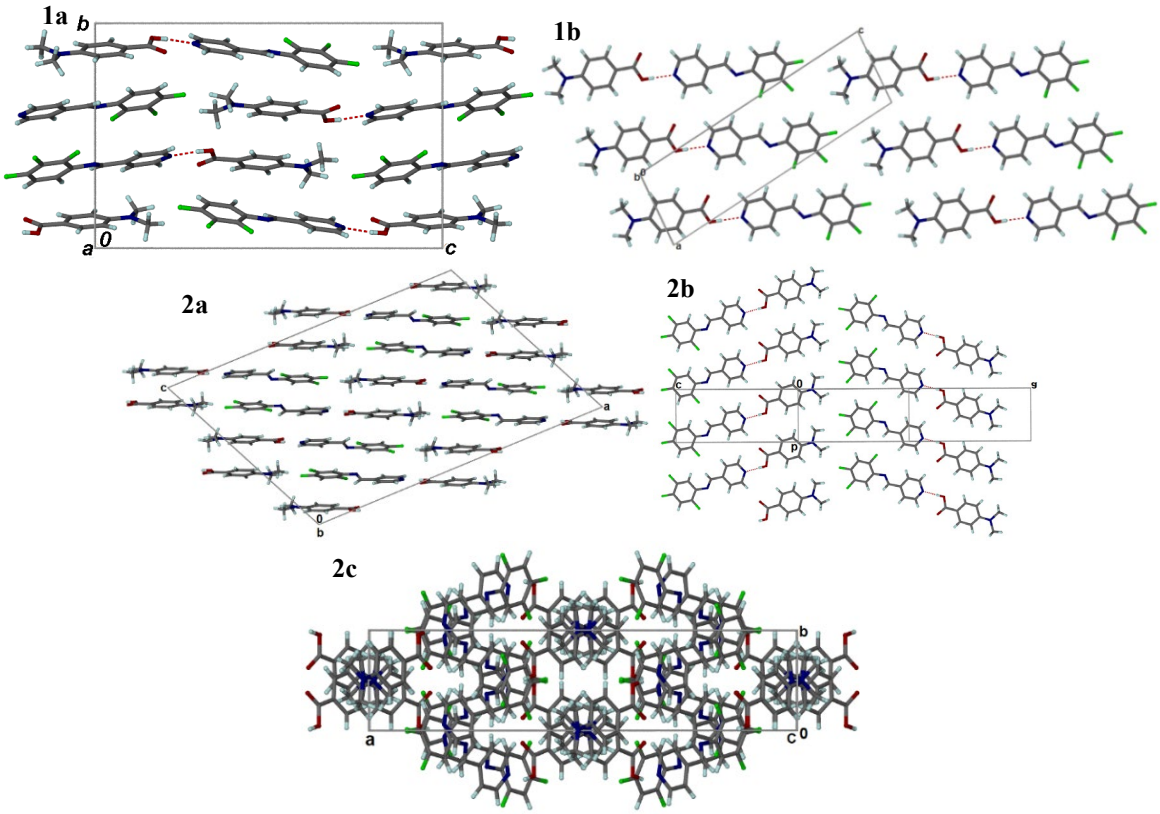

Fig. 7. Packing of molecules ***1*** and ***2*** in the crystal showing parallel and perpendicular views of the 2D planes.

Computational studies

Density functional theory (DFT) calculations were carried out using the M06-2X functional in combination with the 6-31+G** basis set to estimate the interaction energies between selected molecular pairs. The interaction energies were obtained as simple energy differences without additional corrections. This functional was employed because it provides reasonable values for noncovalent interactions, consistent with those reported by other computational tools such as *CrystalExplorer* and *PIXEL*. The molecular pairs analyzed included those participating in O–H···N hydrogen bonds, as well as additional pairs selected based on the predominant intermolecular contacts identified in the crystal structures. The initial identification of these contacts was assisted by intermolecular potential mapping using the "UNI" force field developed by A. Gavezzotti and co-workers [34,35]. The calculated interaction energies for the different molecular pairs are summarized in Fig. 8.

http://dx.doi.org/10.29356/jmcs.v70i1.2508

J. Mex. Chem. Soc. **2026**, *70(1):e2508*
Regular Issue

ISSN-e 2594-0317

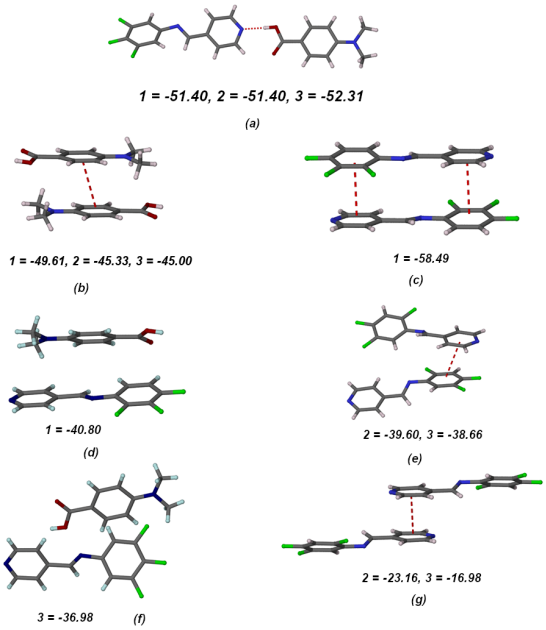

Fig. 8. Illustration of the primary energies between molecules, with the corresponding values in kJ/mol. When several molecules interact, only one is typically shown.

Discussion

The IR spectra for cocrystals ***1–3*** exhibit broad bands around 1950 and 2450 cm^{-1}, indicative of intermolecular O−H···N(py) interactions. Additionally, a band near 1700 cm^{-1} is consistent with carboxylic acid functional groups (see IR spectra in the Supplementary data). The presence of short (~1.22 Å) and long (~1.33 Å) C−O bond distances, corresponding to double and single bonds, respectively, further supports these findings (selected bond distances and angles are presented in Table S2). These spectral features confirm the formation of cocrystals rather than molecular salts, as observed in related studies [36-39]. The detailed spectra of both the imines and their cocrystals are provided in the Supplementary Material.

All three structures feature an O1−H1···N1 hydrogen bond, reinforced by a C2−H2···O2 hydrogen bond, forming a $C^2_2(8)$ synthon. The presence of a C2–H2···O2 hydrogen bond combined with the O1–H1···N1 hydrogen bond explains the alignment of the benzene ring with the planes of the pyridine and trifluorinated aromatic rings. In compounds ***1*** and ***2***, an additional hydrogen bond is observed between the ortho-F atom and the imine hydrogen (C7−H7···F1). However, in ***3***, the absence of the ortho-F atom prevents the formation of this hydrogen bond, and the imine hydrogen (H7) does not engage in any significant bonding, see Fig. 4. This suggests that the C7−H7···F1 interaction arises from geometric proximity and does not play a significant role in the molecular organization. Interestingly, despite the absence of this bond in ***3***, both ***2*** and ***3*** exhibit similar packing arrangements, indicating that other factors play a more critical role in determining the overall crystal structure.

The positioning of the fluorine atoms is crucial for determining the molecular arrangement. In ***1***, the fluorine atoms are positioned on one side of the aromatic ring (positions 2, 3, and 4), leading to centrosymmetric molecular alignment and the formation of 2D planes that stack parallel to one another (Fig. 7**(1b)**). In contrast, in ***2*** and ***3***, the fluorine atoms are distributed on both sides of the ^{F}Ar ring. Although there is an interaction between the ^{F}Ar and pyridine (py) rings, ***2*** and ***3*** also display py···py interactions that are absent in ***1***. These weaker ^{F}Ar···py and py···py interactions result in 2D planes that pack at an angle rather than in parallel (Fig. 7, 2**(b)**, and 2**(c)**). Intermolecular C−H···π and C−X···π interactions are also present in these structures (Supplementary Material).

http://dx.doi.org/10.29356/jmcs.v70i1.2508

J. Mex. Chem. Soc. **2026**, *70(1):e2508*
Regular Issue

ISSN-e 2594-0317

The hydrogen bonds between the Schiff base and benzoic acid have energies of approximately 51–52 kJ/mol and form dimers that significantly influence the short-range molecular arrangement. The π···π interactions between the aromatic rings are the primary forces governing the molecular organization. In ***1***, these interactions are more energetically favorable than the O−H···N hydrogen bond, with the py··· ^{F}Ar π-π interaction exhibiting an interaction energy of −58.49 kJ/mol. The π-π interactions in ***2*** and ***3*** (Fig. 8**(e)**) display different geometries, which influence the lateral packing of these molecules. Additionally, all three structures feature π-π interactions between the aromatic rings of the carboxylic acid groups (Fig. 8**(b)**). Two key interactions are highlighted in Fig. 8**(d)** and 8**(f)**, with energies of -40.80 and -36.98 kJ/mol, respectively. These interactions are not strictly atom-to-atom contacts, and several authors have suggested that they are better understood as molecule-to-molecule interactions. [2].

Conclusions

This study demonstrates that the positioning of fluorine atoms on the aromatic rings of Schiff base cocrystals plays a crucial role in determining the molecular packing and intermolecular interactions. In the 2,3,4-fluorine-substituted aromatic rings, the centrosymmetric π-π interaction between the ^{F}Ar and pyridine (py) rings leads to parallel stacking of molecules. In contrast, when fluorine atoms are positioned on both sides of the ^{F}Ar ring, the packing becomes oblique. We found that π-π stacking interactions, particularly between the pyridine and trifluorinated aromatic rings, are energetically significant and often exceed the strength of O−H···N hydrogen bonds, making them the primary force governing supramolecular organization. Hirshfeld surface analysis revealed the presence of various interactions, including H···N, H···F, and H···O hydrogen bonds, as well as C···C contacts, all of which contribute to the stability and packing of the cocrystals. Computational studies further confirmed the energetic contribution of these interactions. Overall, this research underscores the importance of fluorine atom positioning and provides valuable insights into cocrystal design, highlighting the competitive roles of π-π stacking and hydrogen bonding in determining molecular arrangement and stability.

Acknowledgements

M.H.V and A.D.S.P. thank CONAHCYT for the scholarship. We thank F.J. Pérez-Flores, R.L. Gaviño-Ramírez, and A. Romo-Pérez for their technical assistance. Funding for this research was provided by: Dirección General de Asuntos del Personal Académico, Universidad Nacional Autónoma de México (grant No. PAPIIT: IN224625).

References

1. Karimi-Jafari, M.; Padrela, L.; Walker, G.M.; Croker, D.M. *Cryst. Growth Des.* **2018**, *18*, 10, 6370–6387. DOI: https://doi.org/10.1021/acs.cgd.8b00933.
2. Li, S., Cooper, V.R.; Thonhauser, T.; Lundqvist, B.I.; Langreth, D.C. *J. Phys. Chem. B.* **2009**, *113*, 11166–11172. DOI: https://doi.org/10.1021/JP905765C.
3. Carter-Fenk, K.; Liu, M.; Pujal, L.; Loipersberger, M.; Tsanai, M.; Vernon, R.M.; Forman-Kay, J.D.; Head-Gordon, M.; Heidar-Zadeh, F.; Head-Gordon, T. *J. Am. Chem. Soc.* **2023**, *145*, 24836–24851. DOI: https://doi.org/10.1021/JACS.3C09198.
4. McGaughey, G.B.; Gagné, M.; Rappé, A.K. *J. Biol. Chem.* **1998**, *273,* 15458–15463. DOI: https://doi.org/10.1074/jbc.273.25.15458.
5. Tiekink, E.R.T.; Zukerman-Schpector, J., in: *The Importance of Pi-Interactions in Crystal Engineering*, Wiley, **2012**. DOI: https://doi.org/10.1002/9781119945888.

J. Mex. Chem. Soc. **2026**, *70(1):e2508*
Regular Issue

ISSN-e 2594-0317

6. Jaime-Adán, E.; Hernández-Ortega, S.; Toscano, R.A.; Germán-Acacio, J.M.; Sánchez-Pacheco, A.D.; Hernández-Vergara, M.; Barquera, J.E.; Valdés-Martínez, J. *Cryst. Growth. Des.* **2024**, *24*, 1888–1897. DOI: https://doi.org/10.1021/acs.cgd.3c00910.
7. Ojala,W.H.; Arola,T.M.; Herrera, N.; Balidemaj, B.; Ojala,C.R. *Acta Crystallogr. C.* **2007**, 63, o207–o211. DOI: https://doi.org/10.1107/S0108270107006233.
8. Ojala, W.H.; Smieja, J.M.; Spude, J.M.; Arola, T.M.; Kuspa, M.K.; Herrera, N. *Acta Crystallogr. B.* **2007** *63* 485–496. DOI: https://doi.org/10.1107/S0108768107018034.
9. Ojala, W.H.; Lystad, K.M.; Deal, T.L.; Engebretson, J.E.; Spude, J.M.; Balidemaj, B.; Ojala, C.R. *Cryst. Growth. Des.* **2009**, *9* 964–970. DOI: https://doi.org/10.1021/cg8007443.
10. MacGillivray, L.R. *J. Org. Chem.* **2008**, *73,* 3311–3317. DOI: https://doi.org/10.1021/jo8001563.
11. Sinnwell, M. A.; Baltrusaitis, J.; MacGillivray, L.R. *Cryst. Growth. Des.* **2015**, *15,* 538–541. DOI: https://doi.org/10.1021/cg501571u.
12. Li, C.; Campillo-Alvarado, G.; Swenson, D.C.; MacGillivray, L.R. *CrystEngComm.* **2021**, *23,* 1071–1074. DOI: https://doi.org/10.1039/D0CE01885F.
13. Bučar, D.-K.; Sen, A.; Mariappan, S.V.S.; MacGillivray, L.R. *Chem. Comm*. **2012**, *48* 1790. DOI: https://doi.org/10.1039/c2cc15453f.
14. Sinnwell, M.A.; Groeneman, R.H.; Ingenthron, B.J.; Li, C.; MacGillivray, L.R. *Commun Chem.* **2021**, *4*, 60. DOI: https://doi.org/10.1038/s42004-021-00493-3.
15. Grobelny, A.L.; Rath, N.P.; Groeneman, R.H., *CrystEngComm.* **2018**, *20,* 3951–3954. DOI: https://doi.org/10.1039/C8CE00447A.
16. Mondal, B.; Zhang, T.; Prabhakar, R.; Captain, B.; Ramamurthy, V. *Photochem. Photobiol.* **2014**, 13,1509–1520. DOI: https://doi.org/10.1039/c4pp00221k.
17. Hu, F.; Mi, Y.; Zhu, C.; Abrahams, B.F.; Braunstein, P.; Lang, J. *Angew. Chem., Int. Ed. Engl.* **2018**, *130,* 12878–12883. DOI: https://doi.org/10.1002/ANGE.201806076.
18. Präsang, C.; Nguyen, H.L.; Horton, P.N.; Whitwood, A.C.; Bruce, D.W. *Chem. Comm.* **2008**, 6164. DOI: https://doi.org/10.1039/b811716k.
19. Cariati, E.; Roberto, D.; Ugo, R.; Srdanov, V.I.; Galli, S.; Macchi, V; Sironi, A. *New J. Chem.* **2002**, *26* 13–15. DOI: https://doi.org/10.1039/b107632a.
20. Wong, J.P.-W.; Whitwood, A.C.; Bruce, D.W. *Chem. Eur. J.* **2012**, *18*, 16073–16089. DOI: https://doi.org/10.1002/chem.201201906.
21. Bruce, D.W.; Metrangolo, P.; Meyer, F.; Präsang, C.; Resnati, G.; Terraneo, G.; Whitwood, A.C. *New J. Chem*. **2008**, *32,* 477–482. DOI: https://doi.org/10.1039/B709107A.
22. Jaime-Adán, E.; Germán-Acacio, J.M.; Toscano, R.A.; Hernández-Ortega, S.; Valdés-Martínez, J. *Cryst. Growth. Des.* **2020**, *20*, 2240–2250. DOI: https://doi.org/10.1021/acs.cgd.9b01371.
23. Jaime-Adán, E.; Hernández-Ortega, S.; Toscano, R.A.; Germán-Acacio, J.M.; Sánchez-Pacheco, A.D.; Hernández-Vergara, M.; Barquera, J.E.; Valdés-Martínez, J. *Cryst. Growth. Des.* **2024**, *24,* 1888–1897. DOI: https://doi.org/10.1021/acs.cgd.3c00910.
24. Sánchez-Pacheco, A.D.; Hernández-Vergara, M.; Jaime-Adán, E.; Hernández-Ortega,V; Valdés-Martínez, J. *J Mol Struct* **2021,** 1234. DOI: https://doi.org/10.1016/j.molstruc.2021.130136.
25. Bruker AXS Inc; *APEX 3, SAINT and SADABS*, Wisconcin, Madison, USA, 2007.
26. Sheldrick, G.M. *Acta Crystallogr. Section A.* **2015** *71* 3–8. DOI: https://doi.org/10.1107/S2053273314026370.
27. Sheldrick, G.M. *Acta Crystallogr. C Struct. Chem.* **2015**, *71*, 3–8. DOI: https://doi.org/10.1107/S2053229614024218.
28. Spek, A.L. *J. Appl. Crystallogr.* **2003**, *36,* 7–13. DOI: https://doi.org/10.1107/S0021889802022112.
29. Macrae, C.F.; Sovago, I.; Cottrell, S.J., Galek, P.T.A.; McCabe, P.; Pidcock, E.; Platings, M.; Shields, G.P.; Stevens, J.S.; Towler, M.; Wood, P.A. *J. Appl. Crystallogr.* **2020**, *53* 226–235. DOI: https://doi.org/10.1107/S1600576719014092.
30. Barbour, L.J. *J. Appl. Crystallogr.* **2020**, *53*, 1141–1146. DOI: https://doi.org/10.1107/S1600576720007438.

J. Mex. Chem. Soc. **2026**, *70(1):e2508*
Regular Issue

ISSN-e 2594-0317

31. Spackman, P.R.; Turner, M.J.; McKinnon, J.J.; Wolff, S.K.; Grimwood, D.J.; Jayatilaka, D.; Spackman, M.A. **2021**, *54,* 1006–1011. DOI: https://doi.org/10.1107/S1600576721002910.
32. Spackman, M.A.; Jayatilaka, D.; *CrystEngComm.* **2009**, *11*, 19–32. DOI: https://doi.org/10.1039/b818330a.
33. Spackman, M.A.; McKinnon, J.J. *CrystEngComm.* **2002**, *4*, 378–392. DOI: https://doi.org/10.1039/b203191b.
34. Gavezzotti, A. *Acc. Chem. Res.* **1994***, 27,* 309–314. DOI: https://doi.org/10.1021/ar00046a004.
35. Gavezzotti, A.; Filippini, G. *J. Phys. Chem.* **2002**, *98* 4831–4837. DOI: https://doi.org/10.1021/J100069A010.
36. Aakeröy, C.B.; Rajbanshi, A.; Li, Z.J.; Desper, J. *CrystEngComm*. **2010**, *12*, 4231. DOI: https://doi.org/10.1039/c0ce00052c.
37. Brittain, H.G. *Cryst. Growth. Des.* **2009**, *9*, 2492–2499. DOI: https://doi.org/10.1021/cg801397t.
38. Childs, S.L.; Stahly, V.; Park, A. *Mol. Pharm.* **2007**, *4,* 323–338. DOI: https://doi.org/10.1021/mp0601345.
39. da Silva, C.C.; Guimarães, F.F.; Ribeiro, L.; Martins, V. *Spectrochim. Acta A Mol. Biomol. Spectrosc.* **2016**, *167*, 89–95. DOI: https://doi.org/10.1016/j.saa.2016.05.042.